Japanese Journal of Applied Physics
Vol. 45, No. 6A, 2006, pp. 5035–5038

Effect of Spherical Aberration on Fabrication of Fiber Bragg Gratings

Yoshifumi SUZAKI*, Jun-pei MOHRI, Keisuke NAKAYAMA†, Maki ANDO‡, Kenji SAKAMOTO, Makoto YAMAUCHI[1], Yasuo MIZUTANI[1], Takashi YOKOUCHI and Seiki EJIMA

Department of Advanced Material Science, Faculty of Engineering, Kagawa University, 2217-20 Hayashi-cho, Takamatsu 761-0396, Japan
[1]*Shinko Electric Wire Co., Ltd., 1298-12 Shido, Sanuki, Kagawa 769-2101, Japan*

(Received February 13, 2006; accepted March 15, 2006; published online June 8, 2006)

Cylindrical convex lenses are commonly used in fabricating fiber Bragg gratings (FBGs) by the phase mask method to increase the energy fluence of UV laser light and thereby enhance FBG productivity. We have found that lens aberrations can affect the efficiency of FBG fabrication by this method. Comparisons of the experimental measurements of FBG transmission minimum as a function of fiber position during irradiation by focussed excimer laser light with ray tracing calculations demonstrate the effect of spherical aberration, particularly for lenses with shorter focal lengths.
[DOI: 10.1143/JJAP.45.5035]

KEYWORDS: fiber Bragg grating, optical fiber, lens, aberration

1. Introduction

Because fiber Bragg gratings (FBGs) have very sharp, narrow-band reflection spectra, they are well suited for applications involving narrow-band optical signals, such as optical filters in optical telecommunication systems, fiber laser cavities, and various types of fiber sensors.

FBGs, which have a periodic structure of the refractive index inside the optical fiber in the longitudinal direction, are commonly fabricated by exposing the optical fiber to UV laser light. Because the grating period is very short, on the order of 0.5 μm, irradiation is normally carried out in the interference patterns of UV laser light so that these patterns are transprinted into the optical fibers.

There are two standard methods for generating these interference patterns: the two-beam interference method and the phase mask method.[1)] In the first method, an interference pattern is formed by splitting the incident UV laser beam into two, deflecting the two beams with mirrors and letting them cross each other. The second method uses a phase mask grating; that is, a UV laser beam incident onto the phase mask is diffracted into +1st and −1st order beams that interfere with each other within a short distance from the phase mask, typically less than 1 mm. The optical fiber is placed very close to or in contact with the mask. Although the two-beam interference method has the advantage of allowing FBG production with different grating periods simply by controlling the crossing angle of the two beams, the phase mask method is more common, presumably because of high reproducibility in FBG fabrication owing to the fact that the optical fiber is positioned very close to the mask.

To enhance the efficiency of FBG fabrication by the phase mask method, it is customary to increase the fluence of the incident UV laser light by inserting a plano-convex lens and placing the optical fiber near its focal point. We have found that the optimum position for the optical fiber is not on the optical axis of the plano-convex lens, contrary to our initial expectation. Instead, higher efficiency was obtained by shifting the fiber away from the optical axis of the lens. With the aid of detailed experiments and ray tracing calculations, we demonstrate that this higher efficiency is explained by the spherical aberration of the plano-convex lens that produces a higher energy fluence off axis.

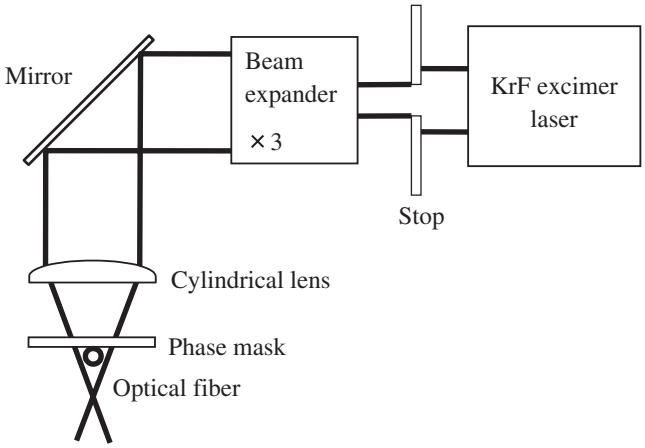

Fig. 1. Illustration of FBG fabrication by phase mask method.

2. Experimental Methods

Our experimental setup is illustrated schematically in Fig. 1.[2)] The excimer laser (Lamda Physik, COMPex-102) delivers up to 240 mJ/pulse at 248 nm with a pulse width of 25 ns at repetition rates of 1–20 Hz. The $8 \times 24\,mm^2$ rectangular output beam is shaped by a $7 \times 7\,mm^2$ stop to select a higher quality uniform portion of the beam. This limits the energy to 60 mJ. After passing through a 3× beam expander, the beam is deflected downward by a mirror and focused by a plano-convex cylindrical lens. A phase mask is mounted in front of the nominal focus of the lens. A bare optical fiber is placed underneath the phase mask at a distance of less than 0.5 mm. We have used two different plano-convex cylindrical lenses (Sigma Koki, fused silica cylindrical lenses F100 and F200), with focal lengths of 87.9 mm (F100) and 176.9 mm (F200), as shown in Figs. 2(a) and 2(b), respectively. The lens parameters are given in Table I. Focal length is defined in the table by its

*E-mail address: suzaki@eng.kagawa-u.ac.jp
†Present address: MicroCraft, Inc., 630-2 Tanaka, Okayama 700-0951, Japan.
‡Present address: Aoi Electronics Co., Ltd., 455-1, Kohzai Minamimachi, Takamatsu 761-8014, Japan.

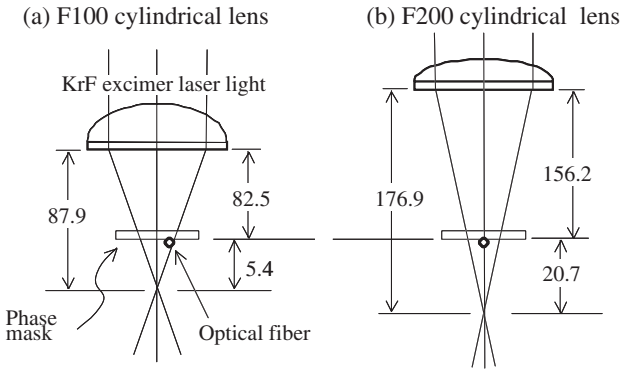

Fig. 2. Optical arrangements of two cylindrical lenses F100 (a) and F200 (b).

Table I. Lens parameters (unit: mm).

Lens type	F100	F200
Focal length	87.9	176.9
Lens thickness	5.0	5.0
Curvature radius	46.0	92.0

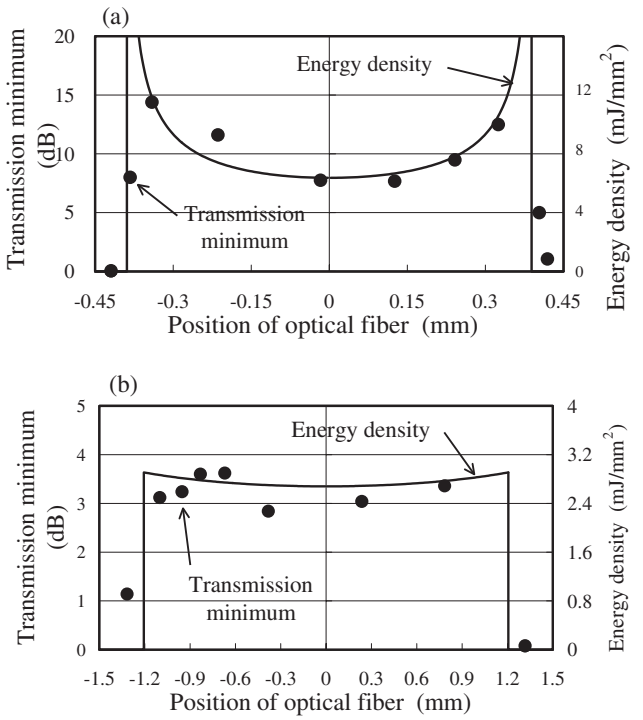

Fig. 3. Transmission minimum of FBGs generated using two different lenses plotted against shift of optical fiber perpendicular to optical axis of lens. The solid lines are ray tracing calculations of the distribution of the energy fluence for the corresponding lenses: (a) F100; (b) F200.

distance from the lens back surface. The beam is focussed in the direction perpendicular to the optical fiber, i.e., in the right-left direction in the plane of Fig. 2. The 21 mm width of the beam as it is incident on the cylindrical lens is reduced to 1–2.5 mm at the position of the optical fiber. The optical fiber is mounted 5.4 mm in front of the focal point in Fig. 2(a) and 20.7 mm in Fig. 2(b).

The optical fiber used here is a standard single mode fiber (Corning SMF-28), with core and cladding diameters of 8.3 and 125 μm, respectively. Prior to the experiment, the fiber was kept under 10 MPa hydrogen gas for ten days for hydrogen loading to increase its sensitivity to UV light. The resin coating of the fiber was removed and the fiber was ultrasonically cleaned just before it was placed underneath the phase mask. The grating period p of the phase mask is 1070.3 nm giving the grating pitch $\Lambda = p/2$ in the fiber core; hence, using the effective refractive index of the optical fiber $n_{\text{eff}} = 1.446$, the FBG central wavelength is expected to be $\lambda_0 = 2n_{\text{eff}}\Lambda = 2n_{\text{eff}}p/2 \sim 1547$ nm.

During FBG fabrication using the shorter-focal-length lens (F100), we noticed that the efficiency of FBG formation is very sensitive to the fiber position relative to the optical axis, in contrast to our initial expectation that the highest efficiency should be obtained on the optical axis. Suspecting that this phenomenon might be a lens aberration effect, we carefully shifted the position of the optical fiber away from the optical axis of the lens and studied how the efficiency of FBG formation depends on the fiber position. We define the efficiency of FBG formation by the transmission minimum attained after a given duration of exposure to the laser light for quantitative comparison.

We normally monitor FBG formation by injecting a broadband light signal from an amplified spontaneous emission (ASE) source (Thorlabs ASE-7701-AP) and by analyzing the signal transmitted through the FBG using an optical spectrum analyzer (Advantest Q8384).

By exposing the optical fiber to the excimer laser light for 30 s, we measured FBG transmission minimum from the optical spectrum. The dependence of transmission minimum on the position of the optical fiber relative to the optical axis of the plano-convex lens is shown by the solid circles in Figs. 3(a) and 3(b), for which the lens configurations correspond to Figs. 2(a) and 2(b), respectively. The positional dependence for the shorter-focal-length lens [F100, Fig. 3(a)] varies strongly, particularly toward the edge of the beam, whereas for the longer-focal-length lens (F200), this dependence is almost uniform. Note that the diameter of the optical fiber is 0.125 mm. The solid curves are energy fluence distributions obtained from the ray tracing calculations discussed in the next section.

3. Theory

The optical geometry for our calculations is shown in Fig. 4. We shall derive the equation of the ray that enters the lens, with the angle of incidence θ_{in}, at position #1 and exits the lens with the exit angle θ_{out} at position #2. At position #1, we have

$$x_1 = R - D - R\cos\theta_{\text{in}}, \quad y_1 = R\sin\theta_{\text{in}} \tag{1}$$

$$\frac{\sin\theta_{\text{in}}}{\sin\theta_{\text{L}}} = \frac{n_{\text{L}}}{n_{\text{air}}}. \tag{2}$$

The equation for the line from #1 to #2 is

$$\frac{y - y_1}{x - x_1} = -\tan(\theta_{\text{in}} - \theta_{\text{L}}), \tag{3}$$

where R is the radius of curvature of the lens surface and D is the thickness of the lens. θ_{L} is the angle of refraction at position #1. Here, n_{L} and n_{air} are the refractive indices of

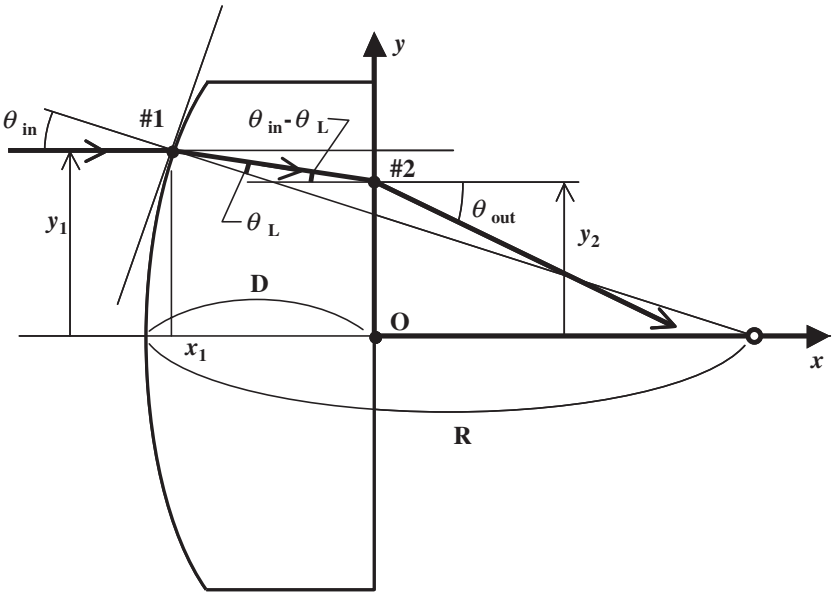

Fig. 4. Illustration of geometry for ray tracing calculations in plano-convex cylindrical lens.

the lens and air, respectively. At the exit position #2, we obtain similar equations, i.e.,

$$x_2 = 0, \quad y_2 = x_1 \tan(\theta_{\text{in}} - \theta_{\text{L}}) + y_1 \tag{4}$$

$$\frac{y - y_2}{x} = -\tan\theta_{\text{out}}, \quad \frac{\sin(\theta_{\text{in}} - \theta_{\text{L}})}{\sin\theta_{\text{out}}} = \frac{n_{\text{air}}}{n_{\text{L}}} \tag{5}$$

and

$$\begin{aligned} y &= -x\tan\theta_{\text{out}} + y_2 \\ &= -x\tan\theta_{\text{out}} + x_1\tan(\theta_{\text{in}} - \theta_{\text{L}}) + y_1. \end{aligned} \tag{6}$$

Substituting x_1 by eq. (1), the equation for the exiting ray becomes

$$\begin{aligned} y = &-x\tan\theta_{\text{out}} \\ &+ (R - D - R\cos\theta_{\text{in}})\tan(\theta_{\text{in}} - \theta_{\text{L}}) + y_1. \end{aligned} \tag{7}$$

Using the above equations, we have traced the paths of paraxial rays incident on the lens with a step size of 1 mm across our beam width. The results are shown in Fig. 5 near the focal point. The lens parameters are those given in Table I, and the refractive index of the lens n_{L} is taken to be 1.508 equal to that for silica glass at the wavelength of the KrF excimer laser (248 nm). The effect of aberration is clearly evident for the shorter-focal-length (F100) lens [Fig. 5(a)], whereas it is negligible for the longer-focal-length (F200) lens [Fig. 5(b)].

The distribution of the energy fluence of the laser light can also be calculated from the equations discussed above as

$$E_3(y) = E_1 \times \frac{\Delta y_1}{\Delta y_3}. \tag{8}$$

Assuming a uniform distribution of the energy fluence of the incident laser light incident on the lens (position #1), i.e., E_1, the distribution $E_3(y)$ beyond the lens can be obtained at any point by determining the paths of a set of rays separated by the small, fixed step size Δy_1 at position #1 in the same way as in Fig. 5 and using eq. (8). The calculated results for the two lenses used in our experiments are shown by the solid lines in Figs. 2(a) and 2(b). These figures show that the calculated energy fluence distributions correlate well with the dependence of FBG transmission minimum on the distance from the optical axis of the focussing lens. This confirms the effect of spherical aberration on the optimum position for FBG production using these lenses.

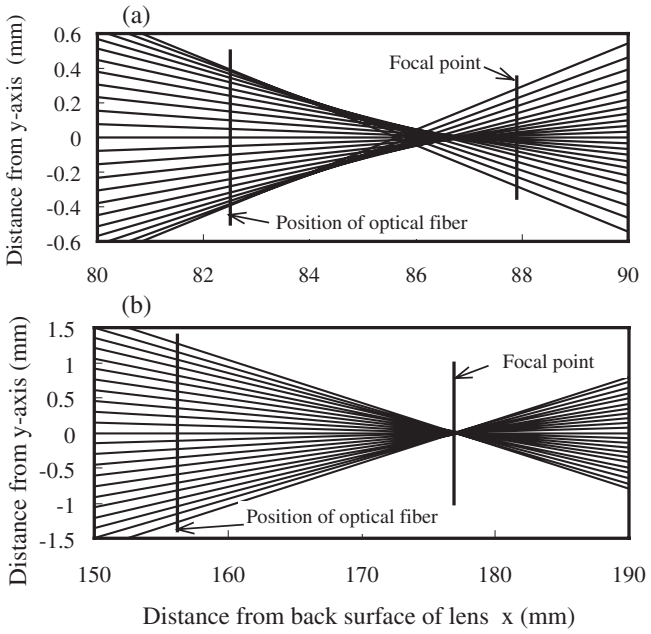

Fig. 5. Calculated ray paths near focal point of two plano-convex cylindrical lenses used in our experiments.

4. Conclusions

In the phase mask method for the fabrication of FBGs by exposing an optical fiber to UV laser light, a cylindrical lens is commonly used to enhance the energy fluence of the laser light. The fiber is mounted near the focal point of the lens to take advantage of the higher fluence. It might be expected that the optimum position for the optical fiber would be on

the optical axis of the lens. On the other hand, we have found that the best position for FBG fabrication is somewhat shifted from the optical axis of the focussing lens. Experimental data on the efficiency of FBG fabrication (defined in terms of grating transmission minimum) were in good agreement with theoretical ray tracing calculations for the lenses employed in these experiments, thus confirming the effect of lens aberration. Thus, the effect of lens aberration on FBG fabrication should be taken into account, particularly when short focal length lenses are used.

Acknowledgements

We thank Dr. H. Iwata of Takamatsu National College of Technology for his kind advice about the lens aberration. We also acknowledge Dr. D. H. McNeill for his careful proofreading of our manuscript.

1) R. Kashyap: *Fiber Bragg Grating* (Academic Press, London, 1999) p. 55.
2) M. Nakamura, C. Komatsu, Y. Masuda, K. Fujita, M. Yamauchi, Y. Mizutani, S. Kimura, Y. Suzaki, T. Yokouchi, K. Nakagawa and S. Ejima: Jpn. J. Appl. Phys. **43** (2004) 147.